Synthesis, X-ray Structural Analysis and Spectroscopic Investigations (IR and ^{31}P MAS NMR) of Mixed Barium/Strontium Fluoroapatites

Abdallah Aissa,[a] Béchir Badraoui,[a] René Thouvenot,*[b] and Mongi Debbabi*[a]

Keywords: Barium / IR spectroscopy / NMR spectroscopy / Strontium / X-ray diffraction

Continuous solid solutions of barium/strontium fluoroapatites $Ba_{(10-x)}Sr_x(PO_4)_6F_2$ ($Ba_{(10-x)}Sr_xFAp$; $0 \leq x \leq 10$) were obtained in an aqueous medium. They were investigated by Rietveld structure-refinement methods using powder X-ray diffraction patterns and by chemical analysis, IR spectroscopy and ^{31}P MAS NMR spectroscopy. Replacement of barium by strontium induces a regular decrease of the lattice constants *a* and *c* according to Vegard's law. The results of the powder-fitting structure refinements indicate a clear preference of strontium for the S(1) site of the apatitic structure. A high-wavenumber shift of the IR absorption bands characteristic of PO_4 internal modes is also observed, in agreement with the diminution of the ionic character of the M–O bonds. For increasing strontium content, a regular δ_{iso} increase is shown in the ^{31}P MAS NMR spectra, from $\delta = 0.91$ ppm for $Ba_{10}FAp$ to $\delta = 3.06$ ppm for $Sr_{10}FAp$. For all mixed Ba/Sr fluoroapatites, the low intensities of the spinning bands reflect the weak ^{31}P chemical-shift anisotropy, in agreement with the low distortion of the PO_4 tetrahedron, as shown by Rietveld refinement.

Introduction

Apatite is a general name for a large family of isomorphous compounds, with the structure belonging basically to the hexagonal space group $P6_3/m$.[1] The general chemical formula is $M_{10}(XO_4)_6Y_2$, where M corresponds to a divalent cation such as Ca^{2+}, Sr^{2+}, Ba^{2+}, Cd^{2+}, or Pb^{2+}, XO_4 is a trivalent anion, essentially PO_4^{3-}, VO_4^{3-} or AsO_4^{3-}, and Y a monovalent anion, like OH^-, F^-, Cl^-, Br^-.[2,3] Furthermore, M^{2+} may be partially replaced by mono- or trivalent cations (Na^+, K^+, Al^{3+}, ...) and XO_4^{3-} may be replaced by tetravalent anions like SiO_4^{4-} and divalent anions like CO_3^{2-} and SO_4^{2-}.

The natural fluoroapatite, $Ca_{10}(PO_4)_6F_2$, is considered as a good structural model for apatitic compounds.[1] The Ca^{2+} cations are located in two nonequivalent crystallographic sites (Figure 1). In each unit cell four Ca(1) atoms, located on the threefold axis, are coordinated by six oxygen atoms as nearest neighbors belonging to the PO_4 group. The site S(1), occupied by Ca(1) atoms, is 4f (symmetry C_3). The other six Ca(2) atoms in the unit cell are coordinated by six oxygen atoms from the PO_4 tetrahedra and by one F^- ion located on the sixfold axis. The site S(2), occupied by Ca(2), is 6h (symmetry C_s). This structure can accommodate a variety of substitutions which affect the physicochemical properties of the materials. In particular, ionic substitutions are involved in dental and bone pathologies, bioceramics for bone implants, pollution by phosphate fertilizers, ion-exchange ability for water treatment and radioactive-waste confinement, as well as in catalytic and luminescent properties.[4,5]

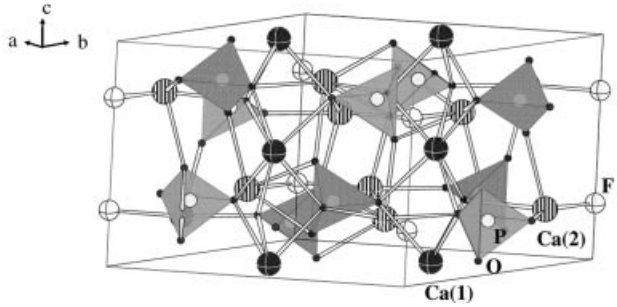

Figure 1. Perspective view of $Ca_{10}(PO_4)_6F_2$ structure

Fluoroapatites are known for the divalent metals Ca, Sr, Ba and Pb,[6–8] and dicationic systems of Sr-, Cd-, and Pb-substituted Ca fluoroapatites have been widely investigated.[9–11] For these systems the limit of miscibility may be correlated to the relative properties of the metals (polarisability, electronegativity and essentially cationic

[a] Laboratoire de Physico-chimie des Matériaux, Ecole Nationale d'Ingénieurs de Monastir,
5019 Monastir, Tunisia
Fax: (internat.) + 216-73-500-514
E-mail: mngdbb@enim.rnu.tn
[b] Laboratoire de Chimie Inorganique et Matériaux Moléculaires, UMR CNRS 7071,
Case courrier 42, Université Pierre et Marie Curie, 75252 Paris Cedex05, France
Fax: (internat.) + 33-1-44273841
E-mail: rth@ccr.jussieu.fr
Supporting information for this article is available on the WWW under http://www.eurjic.org or from the authors.

  DOI: 10.1002/ejic.200400224

Table 1. Fractional atomic coordinates and equivalent thermal parameters, after Rietveld refinement, for the mixed Ba/Sr fluoroapatites (e.s.d. in parentheses)

$Ba_{(10-x)}Sr_xFAp$	Atom	x	y	z	B [Å^2]
Ba_{10} [a]	M(1)	0.3333	0.6667	0.0003(3)	0.4434
	M(2)	0.2391(2)	0.9806(1)	0.2500	0.4859
	P	0.3983(4)	0.3665(5)	0.2500	0.2044
	O(1)	0.341(2)	0.486(3)	0.2500	1.0306
	O(2)	0.576(1)	0.462(3)	0.2500	1.1393
	O(3)	0.339(3)	0.268(1)	0.087(1)	1.7448
	F	0.0000	0.0000	0.2981(7)	2.6703
$Ba_{9.01}Sr_{0.99}$ [b]	M(1)	0.3333	0.6667	0.0017(3)	0.4340
	M(2)	0.2382(1)	0.9800(2)	0.2500	0.4756
	P	0.4016(5)	0.3699(4)	0.2500	0.2001
	O(1)	0.346(2)	0.487(3)	0.2500	1.0086
	O(2)	0.573(3)	0.459(2)	0.2500	1.1148
	O(3)	0.341(2)	0.269(4)	0.089(1)	1.7079
	F	0.0000	0.0000	0.2562(5)	2.6127
$Ba_{6.92}Sr_{3.08}$ [c]	M(1)	0.3333	0.6667	−0.0017(6)	0.4075
	M(2)	0.2364(1)	0.9806(2)	0.2500	0.4471
	P	0.4085(8)	0.3758(6)	0.2500	0.1882
	O(1)	0.351(4)	0.491(3)	0.2500	0.9480
	O(2)	0.583(5)	0.455(2)	0.2500	1.0419
	O(3)	0.346(3)	0.271(2)	0.089(4)	1.6113
	F	0.0000	0.0000	0.2493(6)	2.4345
$Ba_{5.05}Sr_{4.95}$ [d]	M(1)	0.3333	0.6667	−0.0006(4)	0.3992
	M(2)	0.2363(2)	0.9803(1)	0.2500	0.4382
	P	0.4096(6)	0.3769(4)	0.2500	0.1844
	O(1)	0.352(1)	0.494(3)	0.2500	0.9290
	O(2)	0.584(1)	0.454(2)	0.2500	1.0198
	O(3)	0.345(3)	0.271(1)	0.089(1)	1.5802
	F	0.0000	0.0000	0.2521(2)	2.3811
$Ba_{2.92}Sr_{7.08}$ [e]	M(1)	0.3333	0.6667	−0.0025(6)	0.3909
	M(2)	0.2378(2)	0.9863(1)	0.2500	0.4293
	P	0.4038(5)	0.3711(6)	0.2500	0.1807
	O(1)	0.341(3)	0.487(2)	0.2500	0.9100
	O(2)	0.586(3)	0.465(4)	0.2500	0.9974
	O(3)	0.342(2)	0.275(5)	0.084(3)	1.5478
	F	0.0000	0.0000	0.2500	2.3267
$Ba_{1.03}Sr_{8.97}$ [f]	M(1)	0.3333	0.6667	−0.0009(2)	0.3705
	M(2)	0.2382(3)	−0.0162(2)	0.2500	0.4072
	P	0.4017(6)	0.3701(4)	0.2500	0.1714
	O(1)	0.337(1)	0.486(2)	0.2500	0.8629
	O(2)	0.582(1)	0.461(3)	0.2500	0.9433
	O(3)	0.345(2)	0.264(1)	0.079(3)	1.4720
	F	0.0000	0.0000	0.2487(5)	2.1975
Sr_{10} [g]	M(1)	0.3333	0.6667	−0.0008(4)	0.3636
	M(2)	0.2391(1)	0.9848(1)	0.2500	0.3996
	P	0.3980(5)	0.3663(3)	0.2500	0.1682
	O(1)	0.332(2)	0.482(2)	0.2500	0.8469
	O(2)	0.580(1)	0.462(1)	0.2500	0.9251
	O(3)	0.344(3)	0.262(2)	0.073(3)	1.4455
	F	0.0000	0.0000	0.2514(3)	2.1542

[a] a = 10.1611(2) Å, c = 7.7322(1) Å, R_p = 5.3, R_{Wp} = 6.9. The pattern R factor, R_p, is defined as $R_p = 100\{|Y_{oi} - Y_{ci}|/Y_{oi}\}$. The weighted pattern R factor, R_{Wp}, is defined as $R_{Wp} = 100\{W_i(Y_{oi} - Y_{ci})^2/W_i(Y_{oi})^2\}^{1/2}$. [b] a = 10.1074(3) Å, c = 7.6896(2) Å, R_p = 3.9, R_{Wp} = 5.4. [c] a = 10.0562(5) Å, c = 7.5939(5) Å, R_p = 5.6, R_{Wp} = 7.4. [d] a = 9.9288(5) Å, c = 7.4893(6) Å, R_p = 3.6, R_{Wp} = 4.7. [e] a = 9.8581(6) Å, c = 7.3590(4) Å, R_p = 6.5, R_{Wp} = 7.2. [f] a = 9.7636(3) Å, c = 7.3258(1) Å, R_p = 3.6, R_{Wp} = 4.9. [g] a = 9.7211(2) Å, c = 7.2869(1) Å, R_p = 5.1, R_{Wp} = 8.4.

size).[12,13] The lattice parameters of these mixed apatites decrease with increasing content of the smaller metal cation, and in the case of the Ca/Sr and Ca/Pb systems the results of powder pattern fitting refinement indicate a clear preference of Ca^{2+} for the site S(1) of the apatitic structure. On the contrary, for Ca/Cd fluoroapatites, the smaller Cd^{2+} cations prefer the S(2) site; this can be explained by a good affinity of cadmium to fluorine. To the best of our knowledge, no other mixed divalent-metal fluoroapatites have been reported.

In this paper we report the synthesis in aqueous medium and the chemical analysis of a continuous series of mixed strontium/barium fluoroapatites; the results of powder fitting structure refinement are discussed in relation with the spectroscopic data (IR and ^{31}P MAS NMR).

Results

X-ray Analysis

The results of X-ray diffraction pattern identification for all products $Ba_{(10-x)}Sr_x(PO_4)_6F_2$ (hereafter $Ba_{(10-x)}Sr_xFAp$; $0 \leq x \leq 10$) indicate that the samples are constituted of a single apatitic phase.

The structural analysis by Rietveld methods for seven samples gave the following formulae: $Ba_{10}FAp$, $Ba_{9.01}Sr_{0.99}FAp$, $Ba_{6.92}Sr_{3.08}FAp$, $Ba_{5.05}Sr_{4.95}FAp$, $Ba_{2.92}Sr_{7.08}FAp$, $Ba_{1.03}Sr_{8.97}FAap$ and $Sr_{10}FAp$. The results of the refined structural parameters for these samples are reported in Table 1. The stoichiometry of these samples is close to that of the synthesis and agrees very well with the chemical analysis (Table 2). Therefore, to simplify, from now onwards the samples will be named as $Ba_{(10-x)}Sr_xFAp$ where x corresponds to the stoichiometry of the synthesis.

The progressive replacement of barium by strontium leads to a slight decrease in the crystallographic parameters a and c; the variations are linear and obey Vegard's law[14] according to the following Equations.

$a = (10.173 - 0.045x)$ Å; $\sigma(a) = 4.5 \times 10^{-2}$ Å
$c = (7.726 - 0.045x)$ Å; $\sigma(c) = 2.3 \times 10^{-2}$ Å
$V = (691.4 - 9.6x)$ Å^3; $\sigma(V) = 0.7$ Å^3

As a typical comparison between the observed and calculated profiles the final plot for Ba_5Sr_5FAp is displayed in Figure 2.

The structural refinement shows that strontium occupies both the S(1) and S(2) sites of the apatitic structure. However, the occupancy in S(1) is always higher than expected from the statistical distribution, as shown in Figure 3 and in Table 3.

The bond lengths and angles for the two metal environments, obtained by DIAMOND,[15] and the distortion indexes of the phosphate tetrahedron calculated by Baur relations,[16] are reported in Table 4. The M−M, M−O, and M(2)−F distances decrease with increasing strontium content and the distortion indexes of the mixed phases are slightly larger than those of the limiting phases.

Table 2. Strontium substitution (atom-%) in mixed Ba/SrFAp (e.s.d. in parentheses)

$Ba_{(10-x)}Sr_xFAp$	Sr(1)/[Sr(1) + Ba(1)]	Sr(1)/[Sr(1) + Sr(2)]	Sr(2)/[Sr(2) + Ba(2)]	Sr/(Sr + Ba)[a]	Sr/(Sr + Ba)[b]
$Ba_{9.01}Sr_{0.99}FAp$	21.9(2)	88.0(2)	1.9(1)	9.9(2)	9.2(5)
$Ba_{6.92}Sr_{3.08}$ FAp	67.22(2)	84.4(3)	8.3(3)	30.8(4)	31.2(2)
$Ba_{5.05}Sr_{4.95}FAp$	81.0(3)	65.3(5)	28.5(5)	49.5(1)	48.5(1)
$Ba_{2.92}Sr_{7.08}$ FAp	90.5(3)	51.1(3)	57.7(4)	70.8(2)	71.6(5)
$Ba_{1.03}Sr_{8.97}FAp$	97.7(1)	43.5(2)	84.4(5)	89.7(2)	91.8(1)

[a] Rietveld refinement. [b] Chemical analysis.

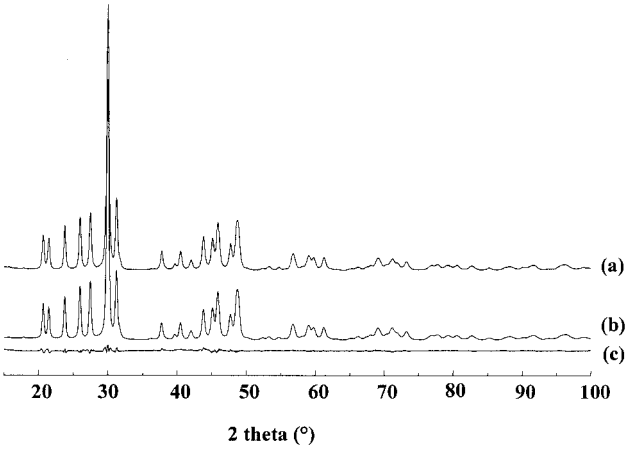

Figure 2. Comparison of the observed [curve (a)] and calculated [curve (b)] powder-diffraction patterns of Ba_5Sr_5FAp; curve (c) is the difference profile

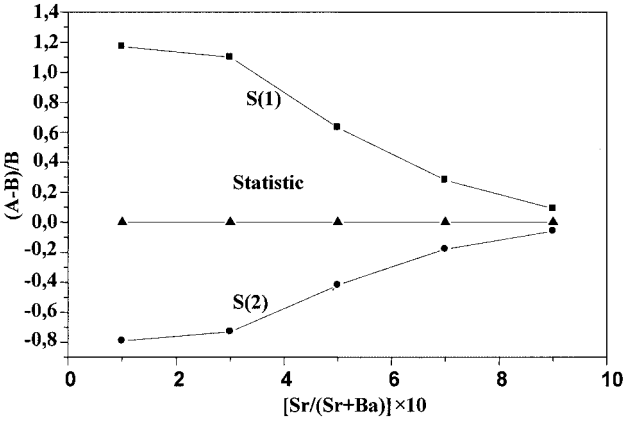

Figure 3. Distribution of strontium between the S(1) and S(2) crystallographic sites

Infrared Absorption Spectroscopy

The infrared spectra of the mixed fluoroapatites present the characteristic absorption bands (stretching and bending) of the PO_4^{3-} group and a band at about 300 cm^{-1} assigned to an M_3-F "ν_3-type stretching "of the 2[M_3-F] sublattice.[17] All IR data are displayed in Table 5 and two typical spectra are presented in the Supporting Information. The progressive replacement of the barium ions by strontium induces a regular shift of all the absorption bands towards greater wavenumbers (Figure 4). Furthermore there is a splitting of the ν_3-[M_3-F] band into two or three components; this effect is markedly pronounced for the intermediate phases, from Ba_6Sr_4FAp to Ba_1Sr_9FAp.

^{31}P Solid-State NMR Analysis

The ^{31}P MAS NMR spectra of the whole series of mixed Ba-SrFAp's are depicted in Figure 5 and the data are given in Table 6. For increasing Sr content, the isotropic signal (δ_{iso}) shows a regular shift towards high frequency between the two limiting phases $Ba_{10}FAp$ (δ_{iso} = 0.91 ppm) and $Sr_{10}FAp$ (δ_{iso} = 3.06 ppm; Figure 6). The low intensity of the spinning side bands (SSB) even at low spinning rate (2 kHz) indicates low chemical-shift anisotropy (CSA) of the phosphorus nucleus; this prevents the determination of the chemical shift tensor components by the classical analysis of the SSB intensity.[18]

As for the Sr/Pb hydroxyapatite system, only one isotropic signal is observed whatever the strontium content. However, for the mixed phases this signal appears complex and contains many components. Despite the weak amplitude of variation of δ_{iso}, numeric simulation allows the decomposition of the isotropic resonance into separate signals, corresponding to different phosphate environments (Figure 7). For the phases with low content of either Sr or Ba (x = 1, 8, 9), the decomposition allows the evaluation of

Table 3. Refinement occupancy compared with the statistic distribution for strontium in the two metal sites S(1) and S(2) of Ba/Sr fluoroapatites

$Ba_{10-x}Sr_xFAp$	Refinement distribution (A)		Statistic distribution (B)		(A − B/B)	
	S(1)	S(2)	S(1)	S(2)	S(1)	S(2)
Ba_9Sr_1FAp	0.87	0.12	0.40	0.59	+1.17	−0.79
Ba_7Sr_3FAp	2.59	0.49	1.23	1.85	+1.10	−0.73
Ba_5Sr_5FAp	3.23	1.72	1.98	2.97	+0.63	−0.42
Ba_3Sr_7FAp	3.62	3.46	2.83	4.25	+0.28	−0.18
Ba_1Sr_9FAp	3.90	5.07	3.59	5.38	+0.09	−0.06

Table 4. Bond lengths, bond angles and PO_4 tetrahedron distortion indices in mixed Ba/Sr fluoroapatites (e.s.d. in parentheses)

	Ba_{10}FAp	Ba_9Sr_1FAp	Ba_7Sr_3FAp	Ba_5Sr_5FAp	Ba_3Sr_7FAp	Ba_1Sr_9FAp	Sr_{10}FAp
P−O(1)	1.57(4)	1.54(4)	1.54(3)	1.53(1)	1.55(2)	1.55(3)	1.54(1)
P−O(2)	1.55(5)	1.50(3)	1.49(6)	1.51(5)	1.52(3)	1.53(1)	1.53(2)
P−O(3)(*)	1.53(5)	1.52(4)	1.53(4)	1.52(3)	1.52(4)	1.53(5)	1.53(2)
P−O mean	1.55	1.52	1.52	1.52	1.53	1.53	1.53
O(1)−O(2)	2.51(5)	2.45(1)	2.53(5)	2.53(4)	2.41(6)	2.53(1)	2.51(2)
O(1)−O(3)(*)	2.53(2)	2.50(2)	2.49(3)	2.49(5)	2.53(7)	2.53(2)	2.52(8)
O(2)−O(3)(*)	2.55(1)	2.49(4)	2.46(2)	2.47(3)	2.49(3)	2.48(3)	2.49(1)
O(3)−O(3)	2.51(1)	2.46(6)	2.44(1)	2.41(1)	2.48(2)	2.49(6)	2.52(6)
O−O mean	2.53	2.48	2.48	2.47	2.49	2.51	2.51
O(1)−P−O(2)	107.1(2)	107.1(2)	111.2(4)	112.2(2)	112.(1)	110.6(5)	109.2(2)
O(1)−P−O(3)(*) (×2)	109.1(2)	109.4(4)	108.1(2)	109.3(2)	108.4(1)	110.4(5)	110.3(1)
O(2)−P−O(3)(*)	110.9(6)	111.2(1)	110.8(6)	109.5(1)	110.1(2)	108.3(4)	108.2(2)
O(3)−P−O(3)	109.5(7)	108.4(5)	106.8(2)	104.9(4)	107.0(3)	108.7(2)	110.6(3)
O−P−O mean	109.4	109.4	109.3	109.2	109.4	109.4	109.5
DI(P−O)	0.0084	0.007	0.010	0.006	0.007	0.003	0.0018
DI(O−P−O)	0.0047	0.007	0.010	0.011	0.012	0.008	0.0083
DI(O−O)	0.0096	0.010	0.015	0.013	0.013	0.009	0.0036
M(1)−O(1)(*) (×3)	2.69(2)	2.68(4)	2.59(2)	2.61(5)	2.55(3)	2.56(1)	2.56(2)
M(1)−O(2)(*)	2.73(3)	2.73(4)	2.67(5)	2.56(6)	2.59(1)	2.56(4)	2.57(6)
M(1)−O(3)(*)	3.13(3)	3.11(5)	3.08(5)	3.01(3)	2.99(2)	2.92(1)	2.91(3)
M(1)−O mean	2.85	2.84	2.78	2.72	2.71	2.68	2.68
M(2)−O(1)	2.91(1)	2.92(6)	2.93(1)	2.94(3)	2.82(5)	2.79(6)	2.75(2)
M(2)−O(2)	2.64(2)	2.65(2)	2.67(3)	2.66(3)	2.54(6)	2.55(4)	2.52(4)
M(2)−O(3) (*)	2.70(7)	2.71(2)	2.72(5)	2.65(5)	2.58(2)	2.54(2)	2.50 (3)
M(2)−O(3) (*)	2.86(2)	2.85(3)	2.85(6)	2.79(2)	2.78(4)	2.70(1)	2.68 (2)
M(2)−O mean	2.78	2.78	2.79	2.75	2.68	2.63	2.61
M(2)−F	2.53	2.51	2.47	2.45	2.41	2.41	2.40
M(2)−M(2)	4.39(1)	4.35(6)	4.30(2)	4.24(4)	4.18(1)	4.17(3)	4.16(2)
M(1)−M(2)	4.23(5)	4.20(1)	4.18(1)	4.14(2)	4.10(6)	4.08(6)	4.07(8)
M(1)−M(1)	3.87(2)	3.82(4)	3.77(2)	3.75(4)	3.67(5)	3.65(4)	3.63(5)

(*) Replicated by symmetry: $DI(PO)=\frac{(\sum_{i=1}^{4}|PO_i-PO_m|)}{4PO_m}$; $DI(OO)=\frac{(\sum_{i=1}^{6}|OO_i-OO_m|)}{6OO_m}$; $DI(OPO)=\frac{(\sum_{i=1}^{6}|OPO_i-OPO_m|)}{6OPO_m}$

Table 5. Infrared band positions [cm^{-1}] for mixed Ba/Sr fluoroapatites

Sample	ν_1	ν_2	ν_3	ν_4	ν_3 (M_3−F)
Ba_{10}FAp	934	444	1005, 1026, 1055	553, 573, 581	293
Ba_9Sr_1FAp	936	445	1007, 1034, 1059	554, 571, 582	295
Ba_7Sr_3FAp	939	448	1010, 1053, 1067	555, 573, 584	301
Ba_6Sr_4FAp	941	450	1013, 1055, 1071	556, 574, 586	301, 307
Ba_5Sr_5FAp	943	451	1015, 1057, 1073	557, 576, 588	301, 309
Ba_4Sr_6FAp	943	453	1016, 1061, 1074	558, 578, 588	297, 312
Ba_3Sr_7FAp	945	455	1018, 1063, 1076	559, 579, 589	301, 322
Ba_2Sr_8FAp	947	456	1019, 1065, 1077	559, 579, 590	304, 314, 322
Ba_1Sr_9FAp	948	457	1022, 1067, 1078	560, 581, 592	291, 314
Sr_{10}FAp	951	458	1026, 1069, 1080	561, 582, 594	322

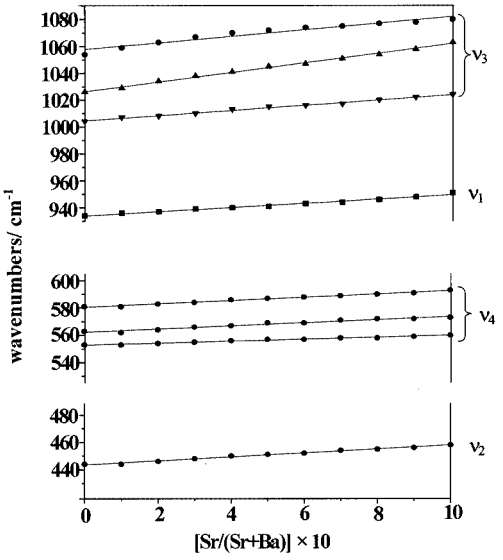

Figure 4. Evolution of the wavenumbers of the PO_4 IR absorption modes as a function of the strontium content

the respective populations of the phosphate sites (Table 7).

For all compositions, the static ^{31}P NMR spectra are quite symmetric, as can be seen in a typical plot (Figure 8); they exhibit a pseudo-Gaussian shape with full width at half maximum (fwhm) of about 14 ppm. The shape of the static spectrum is likely essentially determined by dipolar ^{31}P-^{19}F interactions.

Discussion

The results of this study indicate that the small difference between the cationic radius of Ba^{2+} (1.48 Å) and Sr^{2+} (1.32 Å)[19] allows the formation of a continuous solid solution of barium and strontium fluoroapatites. The replacement of barium in the apatitic structure by the smaller strontium cation induces, as expected, a linear decrease of the lattice

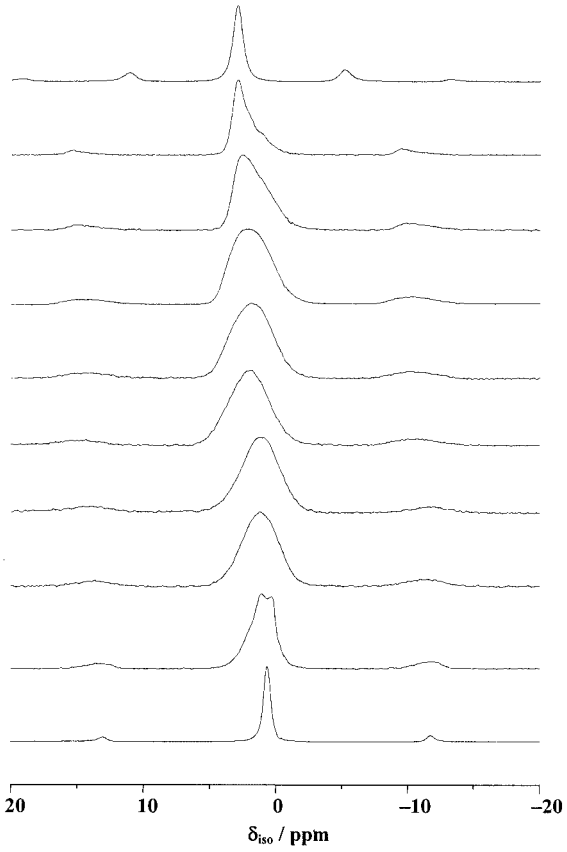

Figure 5. Part of the 162 MHz ^{31}P MAS spectra of the monocationic and mixed Ba/Sr fluoroapatites, showing only the isotropic signal and the spinning side bands; from bottom to top: $Ba_{10}FAp$ (spinning rate R_0 = 2 kHz, number of scans N_s = 1056), Ba_9Sr_1FAp (R_0 = 2 kHz, N_s = 104), Ba_7Sr_3FAp (R_0 = 2 kHz, N_s = 112), Ba_6Sr_4FAp (R_0 = 2 kHz, N_s = 80), Ba_5Sr_5FAp (R_0 = 2 kHz, N_s = 80), Ba_4Sr_6FAp (R_0 = 2 kHz, N_s = 88), Ba_3Sr_7FAp (R_0 = 2 kHz, N_s = 560), Ba_2Sr_8FAp (R_0 = 2 kHz, N_s = 64), Ba_1Sr_9FAp (R_0 = 2 kHz, N_s = 80), $Sr_{10}FAp$ (R_0 = 1.3 kHz, N_s = 272)

Table 6. ^{31}P solid-state NMR spectroscopic data for mixed Ba/Sr fluoroapatites

Samples	δ_{iso} [ppm]	$\Delta_{1/2}$ [ppm]	$\Delta_{1/2static}$ [ppm]
$Ba_{10}FAp$	0.91	0.65	13.5
Ba_9Sr_1FAp	1.2	1.85	14.82
Ba_7Sr_3FAp	1.73	3.18	14.49
Ba_6Sr_4FAp	2.01	3.30	13.81
Ba_5Sr_5FAp	2.2	3.47	13.54
Ba_4Sr_6FAp	2.44	3.61	14.04
Ba_3Sr_7FAp	2.61	3.52	14.75
Ba_2Sr_8FAp	2.83	3.07	14.08
Ba_1Sr_9FAp	2.87	1.90	13.74
$Sr_{10}FAp$	3.06	0.92	12.87

parameters. Despite the variation in the cell dimensions there are no dramatic distortions of the PO_4 tetrahedron (Table 4). The geometry of the phosphate anions remains regular (quasi T_d symmetry) with only small variations over the whole series.

Structural refinements by the Rietveld method show that the Sr^{2+} ions are distributed between the two crystallographic sites S(1) and S(2), with a strong preference for the smaller site S(1). This is particularly marked for low Sr concentrations (Figure 3). Moreover, as the metal−metal distances, determined for $Ba_{10}FAp$, differ markedly for the two types of metallic sites [Ba(1)−Ba(1) = 3.87 Å and Ba(2)−Ba(2) = 4.39 Å] the S(1) sites appear more suitable to accommodate small cations. Furthermore, in $Ba_{10}FAp$ the fluorine atom is shifted to the z position close to 0.3, whereas it is about 0.25 for all solid solutions. This displacement can be related to the sole presence of larger cations (Ba^{2+}) at the S(2) site and the weak affinity of the soft acid Ba^{2+} for the hard base F^-.

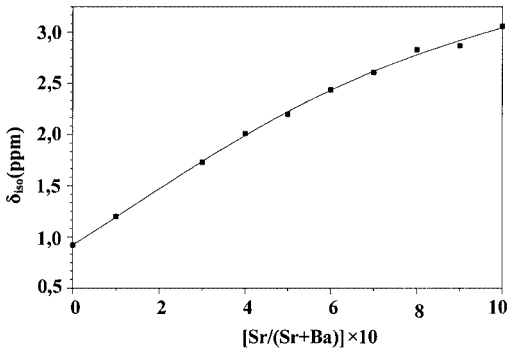

Figure 6. Variation of δ_{iso} as a function of Sr content

The infrared spectra of all mixed fluoroapatites are very similar, especially with respect to the phosphate bands. In particular, the splitting of the triply degenerate ν_3 and ν_4 bands and the intensity of the infrared-inactive bands (for T_d symmetry) ν_1 and ν_2 remain nearly constant over the whole series, in agreement with the minor geometrical perturbations of the PO_4 group (see above). Increasing the strontium content leads, however, to an increase of the frequencies of the PO_4 vibrational modes, and there is a quasi-linear variation of all wavenumbers with the strontium atomic ratio x (Figure 4). As noted by Fowler, who studied pure Ca and Sr hydroxyapatites, this might be due to increased anion−anion repulsions concomitant with decreased lattice dimensions,[17] and also by the higher covalency of the P−O bonds resulting from increased ionicity of the M−O bonds.[13]

According to Fowler,[17] the low-wavenumber bands around 300 cm^{-1} may be assigned to a "ν_3-type stretching" of the M_3−F unit. The multiplicity of these ν_3-[M_3−F] bands observed in the mixed phases can be explained by the various F^- environments — FBa_3, FBa_2Sr, $FBaSr_2$ and FSr_3 — and also by loss of the degeneracy of this E mode by symmetry lowering (D_{3h} to C_{2v}) through metal substitution. This splitting is observed only for the compositions between Ba_6Sr_4FAp and Ba_1Sr_9FAp, when the sites S(2) are significantly occupied by both cations according to the Rietveld refinements (15% Sr/85% Ba for Ba_6Sr_4FAp and 84% Sr/16% Ba in Ba_1Sr_9FAp). Outside this composition range, there is almost exclusively one symmetrical fluorine environment, either FBa_3 or FSr_3, which explains the single ν_3-[M_3−F] absorption band. Two relevant spectra, for

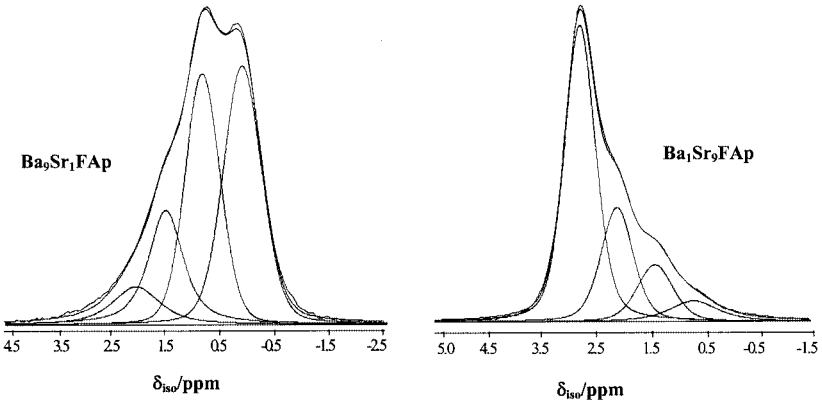

Figure 7. Linefit analysis of the isotropic signal for Ba_9Sr_1FAp and Ba_1Sr_9FAp

Table 7. Relative populations of the various phosphorus environments for Ba_9Sr_1, Ba_2Sr_8 and Ba_1Sr_9 fluoroapatites, from ^{31}P NMR MAS spectra line-fitting analysis

Phosphorus environment	Ba_9Sr_1FAp [a]	[b]	δ_{iso}	Ba_2Sr_8FAp [a]	[b]	δ_{iso}	Ba_1Sr_9FAp [a]	[b]	δ_{iso}
PBa_9	38.74	38	0.21	*	*		*	*	
PBa_8Sr_1	38.74	39	0.90	*	*		*	*	
PBa_7Sr_2	17.22	18	1.52	*	*		*	*	
PBa_6Sr_3	4.46	5	2.25	*	*		*	*	
PBa_5Sr_4	*	*		*	*		*	*	
PBa_4Sr_5	*	*		6.61	7.84	0.86	*	*	
PBa_3Sr_6	*	*		17.62	18.72	1.12	4.46	4	0.45
PBa_2Sr_7	*	*		30.20	29.72	1.98	17.22	18	1.46
PBa_1Sr_8	*	*		30.20	29.93	2.32	38.74	40	2.05
PSr_9	*	*		13.42	13.78	2.98	38.74	38	3.04

[a] Relative amount (%) from statistical formula. [b] Relative amount (%) from line-fitting analysis.

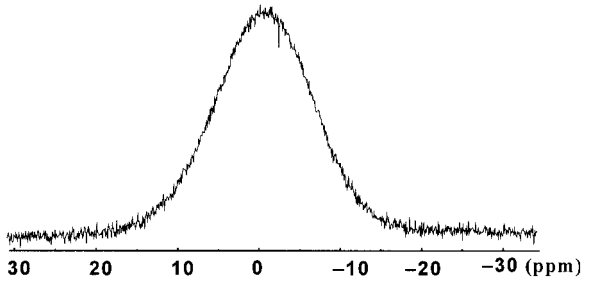

Figure 8. 162 MHz ^{31}P solid-state NMR static spectrum of Ba_5Sr_5FAp

Ba_4Sr_6FAp (38% Sr/Ba 62%) and Ba_5Sr_5FAp (28% Sr/Ba 72%), are given as Supporting Information.

Let us now consider the ^{31}P solid-state MAS NMR results. Solid-state MAS ^{31}P NMR spectra of phosphate compounds generally present a central resonance at δ_{iso} associated with a spinning side-band pattern, characteristic of the chemical shift anisotropy (CSA) of the phosphorus nucleus. In the present case the spectra of all fluoroapatites exhibit low-intensity spinning side-bands, even at moderate spinning rates (Figure 5). This corresponds to a very small CSA interaction, in agreement with the structural analysis, which shows a regular geometry of the phosphate anion for all species (see above).

The limiting phases Ba_{10}FAp and Sr_{10}FAp exhibit a single isotropic resonance, at δ = 0.91 and 3.06 ppm, respectively, in agreement with the equivalence of all phosphate groups in the apatitic structure. For the mixed Ba/Sr fluoroapatites there is a monotonic shift of the position of the isotropic resonance as a function of the strontium content (Figure 6). This regular deshielding of the P nucleus may be correlated to the regular contraction of the lattice parameters.[20]

The variation of δ_{iso} between Ba_{10}FAp and Sr_{10}FAp ($\Delta\delta$ = 2.15 ppm, ca. 350 Hz) is very weak compared to the linewidth of the isotropic signal of these phases (100 and 150 Hz, respectively). Therefore, contrary to what was observed in the Cd/Pb hydroxyapatites system,[21] the isotropic signals associated to different environments of phosphate ions are not resolved in the experimental spectra of the mixed phases. Actually, the ^{31}P resonances of the Ba/Sr fluoroapatites appear as relatively broad signals due to the distribution of the ^{31}P chemical shifts (Figure 5, Table 6). For the phases with low content of either metal — i.e. for x = 1, 8 and 9 — the isotropic resonance has an asymmetrical shape and may be easily decomposed into individual components by using the DOMFIT program.[18] For this analysis we considered that the ^{31}P chemical shift is primarily determined by the cationic environments of the phosphate groups.[22] In the apatitic structure, the phosphorus atoms display nine O−M contacts (Scheme 1). For the nine oxygen−metal contacts around each P atom, neglecting the incidence of the relative positions of Ba and Sr, one expects therefore 10 different P environments, noted $PBa_{(9-y)}Sr_y$ (y = 0, 1, ..., 9). Their relative proportions, which depend on the composition of the apatitic phase, are calculated according to

$$p[PBa_{(9-y)}Sr_y] = C_9^y (p_{Ba})^{(9-y)} (p_{Sr})^y$$

where

$$C_9^y = \frac{9!}{y!(9-y)!}$$

is the binomial coefficient, and p_{Ba} and p_{Sr} are the atomic fractions of Ba and Sr, respectively (Supporting Information). Considering that P environments with less than about 5% abundance would not contribute to the ^{31}P isotropic signal, we can nicely simulate the spectra of Ba_9Sr_1FAp and Ba_1Sr_9FAp with four components (Figure 7). The decomposition of the isotropic signals for these phases give populations of the PO_4 environments close to the statistic weight obtained from their chemical composition (Table 7). From Figure 7, it appears that the linewidth of the individual $PBa_{(9-y)}Sr_y$ resonances increases as y increases (or decreases) towards 0.5. Moreover for "reverse" compositions, strontium-rich environments give broader resonances than their barium-rich analogues (compare Figure 7, right and left). Actually, according to Scheme 1, each $PBa_{(9-y)}Sr_y$ motif corresponds to various slightly different P environments, depending on the relative positions of Ba and Sr in the metallic sites. This may result in subtle variations in ^{31}P chemical shifts and finally in a broader signal than for the single environments PBa_9 and PSr_9. Of course, maximal broadening is expected for the PBa_5Sr_4 and PBa_4Sr_5 motifs. For small y values, corresponding to barium-rich samples, preferential location of strontium at S(1) leads to less-numerous $PBa_{(9-y)}Sr_y$ environments than for the reverse composition $PBa_ySr_{(9-y)}$.

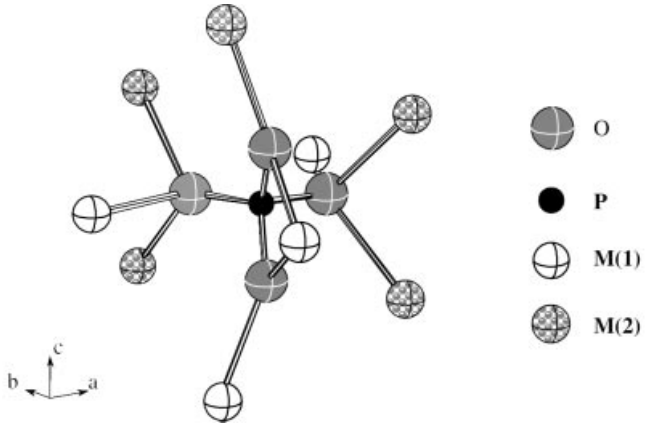

Scheme 1. The cationic environment of the phosphate group in apatitic structure

A more puzzling observation is that the individual lines of the various $PBa_{(9-y)}Sr_y$ motifs shifts more strongly through Ba/Sr substitution (up to 1 ppm, Table 7) than the experimentally observed isotropic signal (mean value of the shift about 0.2 ppm, Table 6 and Figure 6).

Moreover, whereas $\delta_{iso}(PSr_9)$ remains nearly constant (within the accuracy) in Ba_2Sr_8FAp (+2.98 ppm), Ba_1Sr_9FAp (+3.04 ppm) and $Sr_{10}FAp$ (+3.06 ppm), PBa_9 in Ba_9Sr_1FAp (+0.21 ppm, Table 7) is significantly shielded with respect to the same motif in the "pure" phase $Ba_{10}FAp$ (+0.91 ppm, Table 6). Even more surprisingly, PBa_3Sr_6 (in Ba_1Sr_9FAp) and PBa_4Sr_5 (in Ba_2Sr_8FAp) are shielded with respect to PBa_9 in $Ba_{10}FAp$. From all these observations it appears that the ^{31}P isotropic chemical shifts (and linewidths) of the $PBa_{(9-y)}Sr_y$ environments depend significantly on the composition of the apatitic phase; therefore the δ_{iso} values reported in Table 7 cannot be transferred for further simulations.

At variance with the hydroxyapatites,[23] the full width at half maximum ($\Delta\nu_{1/2}$) for the static signal does not change significantly throughout the whole series (14 ± 1 ppm, Table 6). As the P−F dipolar interaction is likely the dominant interaction, the quasi-invariance of $\Delta\nu_{1/2}$ for fluoroapatites shows that the P−F dipolar interaction does not vary when substituting Sr for Ba, in agreement with the P−F distances remaining always of the order of 3.7 Å. By contrast, for hydroxyapatites of space group $P6_3/m$ the statistical orientation of the OH^- ions gives different P−H distances and therefore different dipolar P−H interactions.

Conclusions

Barium strontium fluoroapatites form a continuous series of solid solutions. Structure refinements indicate a clear preference of strontium for the S(1) site of the apatitic structure. Despite the weak amplitude of variation of δ_{iso}, decomposition of the isotropic ^{31}P MAS-NMR resonance into separate signals, corresponding to different phosphate environments, was done for the phases with low content of either Sr or Ba.

Experimental Section

Synthesis: All chemicals, $Ba(CH_3CO_2)_2$, $Sr(NO_3)_2$, NH_4F, and $(NH_4)_2HPO_4$ were of reagent grade (Prolabo, 99% purity) and used without further purification. The mixed barium and strontium fluoroapatites $Ba_{(10-x)}Sr_xFAp$, with x ranging from 0 to 10, were obtained by a double decomposition method.[24,25] This method consists of the preparation in aqueous medium from a solution containing the two metallic cations (A) and a solution of phosphate and ammonium fluoride (B). Concentrations of the solutions in barium, strontium and phosphate ions correspond to the stoichiometry of the desired apatite. A mixture of barium acetate and strontium nitrate, with a total concentration of metal cations of 0.2 M (solution A, 250 mL) and 0.2 M ammonium dihydrogen phosphate solution (solution B, 150 mL) were prepared. Solution A was added dropwise to solution B, maintained at boiling temperature, under nitrogen. The pH of the slurry was maintained at approximately 11 by regular addition of small amounts of ammonia (d = 0.89; 28% aqueous solution). The resulting solid phase was kept in contact with the mother solution at boiling temperature for 1 h. The precipitate was then filtered, washed with hot distilled water, dried at 100 °C for 12 h and calcined at 500 °C for 4 h to improve its crystallinity. The compounds thus obtained were submitted to XRD, chemical analysis, IR spectroscopy and ^{31}P MAS NMR analyses.

Chemical Analyses and Instrumental Methods: Barium and strontium contents were determined with a Perkin−Elmer 3110 atomic absorption spectrophotometer. Phosphorus was determined colorimetrically as phosphovanadomolybdate, by measurement of its absorbance at 430 nm.[26] Fluorine content was determined by potent-

iometry, using an ionometer equipped with a fluoride-specific electrode, at ambient temperature and a pH of about 6. The support electrolyte was a 1 M aqueous solution of sodium citrate. The crystallographic data were collected with a Philips PW1710 diffractometer equipped with a copper anode and a graphite monochromator. The investigated range was from 15 to 100° (2θ), with a step of 0.03° and a counting time of 15 s for each step. IR spectra were obtained from KBr pellets (1 mg sample and 300 mg KBr) with a Bio-Rad FTS 6000 IRFT spectrophotometer in the range 4000−200 cm^{-1}, with a spectral resolution of 4 cm^{-1}. The NMR experiments were performed on powdered samples at room temperature with a Bruker MSL400 spectrometer (9.4 T) operating at 162 MHz. A Doty probehead equipped with 4-mm (diameter) rotors was used for MAS spinning rates up to 6.5 kHz. The spinning rate was monitored by a Bruker pneumatic unit, allowing the control of bearing and drive-inlet air pressure. The spectral width was 45 kHz (280 ppm). The spectra were acquired using a simple one-pulse sequence with phase cycling (CYCLOPS sequence). Pulse duration was 1 μs, (15° flip angle) and the preacquisition and interpulse delays were 22 μs and 5 s, respectively. The 4 K free-induction decay was zero-filled to the size of 8 K and convoluted with an exponential function (exponential multiplication) using a 10-Hz line-broadening factor. The final digital resolution of the spectrum was 10 Hz (0.07 ppm). A better digital resolution, for more accurate determination of the isotropic chemical shifts (±0.05 ppm), was obtained after 16 K zero-filling and no window function. Chemical shifts are reported with respect to external 85% H_3PO_4 in the IUPAC convention, i.e. positive δ corresponds to a resonance at higher frequency (deshielding) than the reference.

Structural Analysis: Rietveld-method crystal-structure refinements from the powder diffraction data were carried out with the DBWS-9411 program.[27,28] The space group ($P6_3/m$) and the atomic positions of the $Ba_{10}(PO_4)_6F_2$ structure were used as starting data in the refinement. First of all, the scale factor and the background coefficients were refined. The peaks were fitted with a "pseudo-Voigt" function. The half-width of the diffraction peaks as a function of 2θ was evaluated by the Caglioti equation.[29] Successively, the pattern parameters (true 2θ zero, peak widths and their dependence on 2θ, asymmetry parameter, preferred orientation parameter) and the lattice parameters were allowed to vary. Finally, the structural parameters (occupancy factor, atomic coordinates) were refined. No constraint was imposed on the overall strontium content. The two sites S(1) and S(2) were imposed to be fully and complementarily occupied by barium and strontium. The occupancy factors of O and P were assumed as constant, in agreement with the apatite stoichiometry. The fractional atomic coordinates were refined starting from the atomic positions of the two metals. No attempt was made to differentiate the barium positions from strontium ones. Rietveld refinement was performed in several stages, the parameters obtained in each stage being deferred in the following. In the last refinement cycles, all 29 parameters were released. Then, the refined parameters were used as initial model for apatite with barium content immediately lower, and so on. The results of the refinement structural parameters (atomic positions, anisotropic thermal parameters, lattice parameters, reliability pattern factors R_p and weighted factors R_{Wp}) are reported in Table 1, while a comparison between the calculated and observed profiles of Ba_5Sr_5FAp is reported in Figure 2. Table 4 gives interatomic distances and distortion indices of phosphate tetrahedron. The strontium-ion distribution between the two sites and chemical analysis results are gathered in Table 2.

Equivalent thermal parameters

$$B_{eq} = \sum_i \sum_j \beta_{ij} (\vec{a}.\vec{b})$$

are calculated by the relation[30]

$$B_{eq} = 4(a^2\beta_{11} + b^2\beta_{22} + c^2\beta_{33} + ab\beta_{12}\cos(\gamma)/3$$

Further details of the crystal-structure investigation may be obtained from the Fachinformationszentrum Karlsruhe, 76344 Eggenstein-Leopoldshafen, Germany, on quoting the depository number CSD-414240.

Supporting Information (see footnote on the first page of this article): Table giving the relative (theoretical) proportions (%) of $PM_{(9-y)}M'_y$ environments as a function of x in the mixed apatites $M_{(10-x)}M'_x(PO_4)_6F_2$ [or $M_{(10-x)}M'_x(PO_4)_6(OH)_2$] (pale-blue background for proportions higher than 4%); Figure giving infrared spectra of Ba_5Sr_5FAp (top) and Ba_4Sr_6FAp (bottom).

Acknowledgments

We greatly acknowledge financial support from the Direction Générale de la Recherche Scientifique et Technique (Tunisie) and the Centre National de la Recherche Scientifique (France) in the frame of a bilateral join project. NMR measurements were performed at the NMR facility center (SIARE) of the Université Pierre et Marie Curie (Paris).

[1] M. I. Kay, R. A. Young, A. S. Posner, *Nature* **1964**, *204*, 1050−1052.
[2] D. McDonnel, *Apatite, Its Crystal Chemistry, Mineralogy, Utilization, and Geologic and Biologic Occurrences*, Springer, New York, N. Y., **1973**.
[3] G. Wright, G. Montel, *C. R. Acad. Sci., Paris* **1969**, *268C*, 2077−2080, *Chem. Abstr.* **1969**, *71*, 56134.
[4] P. Fourman, P. Royer, *Calcium et tissu osseux − Biologie et pathologie*, Flammarion, Paris, **1970**.
[5] T. Suzuki, Y. Hayakawa, *1st International Congress on Phosphorus Compounds*, Rabat, October 17−21, **1977**, p. 381.
[6] E. L. Belokoneva, E. A. Troneva, L. N. Dem′yanets, N. G. Duderov, N. V. Belov, *Kristallografiya* **1982**, *27*, 793−794; *Chem. Abstr.* **1982**, *97*, 118469.
[7] E. R. Kreidler, F. A. Hummel, *Am. Mineral.* **1970**, *55*, 170−184.
[8] M. Mathew, I. Mayer, B. Dickens, L. W. Schroeder, *J. Solid State Chem.* **1979**, *28*, 79−95.
[9] I. Khattech, M. Jemal, *Thermochim. Acta* **1997**, *298*, 23−30.
[10] A. Nounah, J. L. Lacout, *J. Solid State Chem.* **1993**, *107*, 444−451.
[11] I. Ntahomvukiye, I. Khattech, M. Jemal, *Ann. Chim. (Paris)* **1997**, *22*, 435−446; *Chem. Abstr.* **1998**, *128*, 42893.
[12] A. Hamad, B. Badraoui, M. Debbabi, *J. Soc. Chim. Tunisie* **2003**, *5*, 115−124.
[13] A. Aissa Hamad, B. Badraoui, M. Debbabi, *J. Soc. Alger. Chim.* **2003**, *13*, 131−140.
[14] L. Vegard, *Z. Phys.* **1922**, *9*, 395−410.
[15] K. Brandenburg, *DIAMOND*, Crystal Structure Information System, version 1.2, **1997**.
[16] W. H. Baur, *Acta Crystallogr., Sect. B* **1974**, *30*, 1195−1215.
[17] B. O. Fowler, *Inorg. Chem.* **1974**, *13*, 207−214.
[18] D. Massiot, F. Fayon, M. Capron, I. King, S. Le Calvé, B.

Alonso, J.-O. Durand, B. Bujoli, Z. Gan, G. Hoatson, *Magn. Reson. Chem.* **2002**, *40*, 70−76.
[19] R. D. Shannon, *Acta Crystallogr., Sect. A* **1976**, *32*, 751−767.
[20] M. T. Weller, G. Wong, *J. Chem. Soc., Chem. Commun.* **1988**, 1103−1104.
[21] B. Badraoui, A. Bigi, M. Debbabi, M. Gazzano, N. Roveri, R. Thouvenot, *Eur. J. Inorg. Chem.* **2001**, 1261−1267.
[22] S. Aime, G. Digilio, R. Gobetto, A. Bigi, A. Ripamonti, N. Roveri, M. Gazzano, *Inorg. Chem.* **1996**, *35*, 149−154.
[23] B. Badraoui, A. Bigi, M. Debbabi, M. Gazzano, N. Roveri, R. Thouvenot, *Eur. J. Inorg. Chem.* **2002**, 1864−1870.
[24] A. Bigi, M. Gazzano, A. Ripamonti, E. Foresti, N. Roveri, *J. Chem. Soc., Dalton Trans.* **1986**, 241−244.
[25] A. Bigi, G. Falini, E. Foresti, M. Gazzano, A. Ripamonti, N. Roveri, *J. Inorg. Biochem.* **1993**, *49*, 69−78.
[26] K. P. Quinlan, M. A. De Sesa, *Anal. Chem.* **1955**, *27*, 1626−1629.
[27] H. M. Rietveld, *J. Appl. Crystallogr.* **1969**, *2*, 65−71.
[28] R. A. Young, A. Sakthivel, T. S. Moss, C. O. Paiva-Santos, *J. Appl. Crystallogr.* **1995**, *28*, 366−367.
[29] G. Caglioti, A. Paoletti, F. P. Ricci, *Nucl. Instrum.* **1958**, *3*, 223−228.
[30] M. Hata, K. Okada, S. Iwai, *Acta Crystallogr., Sect. B* **1978**, *34*, 3062−3064.

Received March 21, 2004
Early View Article
Published Online August 13, 2004

